NASA Technical Memorandum 101005

Full-Scale UH-60A Rotor Blade Nonrotating Modal Analysis Shake Test

Robert M. Kufeld and David Nguyen, Ames Research Center, Moffett Field, California

November 1989

National Aeronautics and
Space Administration

Ames Research Center
Moffett Field, California 94035

SUMMARY

This report documents the test procedures and results of a nonrotating modal analysis shake test of a full-scale UH-60A rotor blade. The test was performed at NASA Ames Research Center during April of 1986. Five flatwise, two torsional, and two chordwise modes were measured. The frequencies ranged between 4.35 and 82.44 Hz. The results were compared to the natural frequencies calculated by the Comprehensive Analytical Model of Rotorcraft Aerodynamics and Dynamics simulation program. The results will be used to verify mass and stiffness input data for various simulation programs.

NOMENCLATURE

x	longitudinal coordinate of beam
y	vertical coordinate of beam
E	Young's modulus
I	bending moment of inertia about major axes
t	time
m	mass
w	natural frequency
L	overall length of beam
C	constant of integration
r	integer index for solution

INTRODUCTION

In conjunction with NASA's Modern Technology Rotor (MTR) program (ref. 1), the Black Hawk (UH-60A) Rotor Project Plan (ref. 2), and as suggested by Esculier and Bousman (ref. 3), a nonrotating modal analysis shake test was performed on a full-scale UH-60A rotor blade. The blade used in the test was instrumented with strain gages along the span for the Phase One flight test of the UH-60A MTR program. The data from the shake test includes natural frequencies, mode shapes, and damping ratios.

The results will be used to establish a baseline for comparison with both analytical results and future shake test results on two highly instrumented blades. The highly instrumented blades are currently under fabrication and will be used for Phase Two of the MTR program. One blade will have 242 pressure transducers and 50 temperature sensors installed and the other blade will have a total of 42 strain-gage bridges and 14 accelerometers. It is expected that the addition of these transducers will have a slight effect on the blade's natural frequencies.

This report covers the test setup, the procedures, and the results of the full-scale UH-60A rotor blade nonrotating modal analysis shake test, including comparisons with predicted results utilizing the Comprehensive Analytical Model of Rotorcraft Aerodynamics and Dynamics (CAMRAD) program (ref. 3).

The author would like to recognize the fine work of David Nguyen, who was killed in an automobile accident before this report was completed. David initiated the test and collected all of the data.

TEST SETUP

The test was performed at NASA Ames Research Center in the Engineering Test Laboratory. The blade was suspended from a ceiling support beam using a block-and-tackle pulley system and bungee cords (figs. 1 and 2). The bungee cords were used to simulate a free-free suspension of the blade, and were attached to a bracket which was bolted to the blade using the normal retention bolts of the blade. The bracket was also used as the shaker attachment hard point. The shaker was attached directly to the bracket in the chordwise direction (figs. 3 and 4) to excite the chordwise modes, and was attached to the bracket in the flapwise direction to excite the 4th and 5th flapwise and the 2nd torsional modes. To excite the 1st, 2nd, and 3rd flapwise and 1st torsional modes, the shaker was attached to a moment arm (fig. 5). The use of different excitation methods for the lower flapwise and torsional modes was needed to improve the accuracy of the analysis.

The shaker was supported by a 90° angle plate which was clamped to a vertical steel I-beam near the blade. The shaker was attached to the blade by a force link. The force link has a low flexural stiffness and a high axial compressive stiffness to minimize the bending-moment inputs imposed on the blade (uncorrelated inputs) as it rotates during the input. (Uncorrelated input is any input into the system that is not measured and distorts the analysis.) The steel-wire force link is 2 in. long and 1/16 in. in diameter. Between the bracket and the force link, a load cell was installed to measured the input force of the shaker.

This test configuration was checked for data contamination from a possible uncorrelated input caused by shaker feedback. The exciting force of the shaker could travel back into the vertical I-beam to which it was attached, up the I-beam to the ceiling support beam, then down the bungee cords to the blade. The natural frequencies of the vertical I-beam were measured and found to be considerably above the excitation band of interest. From this test, it was concluded that any feedback from the vertical I-beam would be negligible.

Figure 6 is a schematic of the test setup. The shaker and the blade are shown in the chordwise mode of excitation. Signals for driving the electrodynamic shaker originate from the signal generator, which is built into the signal analyzer. These signals were amplified by a power amplifier and fed to the shaker. A piezoelectric load cell attached at the driving point of the blade measured the applied force, which was

then fed to the signal analyzer via a charge amplifier. A movable piezoelectric accelerometer was used to measure the response of the blade at the various node points. The signal from the accelerometer was fed through an amplifier to the signal analyzer, which computed the frequency response functions (FRF) of the two signals. The analyzer had a built-in anti-aliasing filter and a signal generator which performed a discrete sinewave sweep to minimize the timelag between data processing and sweep rate which can impair the data quality. The analyzer did not have full modal analysis capability, therefore the measured FRF values were stored on magnetic disk for further analysis by modal analysis software.

The movable accelerometer was attached to the blade using adapter blocks. The adapter blocks were shaped to match the contour of the blade and were attached to the blade surface using zinc chromate, a sticky, claylike material that allows the accelerometer to be readily moved to the various measurement locations.

PROCEDURES

The first step of the test was to determine the input force level to be used during the shake test. To do this, FRFs were measured while varying the input force level. Figures 7 and 8 show the results of the input force variation on the FRF. It can be seen that the FRF becomes constant at a force level of about 1 lb. This force level was used throughout the test. One measure of a linear system is a constant FRF with increasing input force level. If the force level is too low, the FRF will not be constant with increasing force level because the structure will have insufficient energy to participate fully in the response. If the force level is too high, the structure will have large deflections and again have a varying FRF with increasing force level caused by nonlinear deflections. Exciting the system in the linear range was important because of the uses of a linear analysis.

Another check was made to verify the linearity of the system by examining the FRF with respect to the Maxwell/Betti reciprocity criterion. This criterion states that H_{ij} (the FRF measured at degree of freedom (DOF) i due to excitation at DOF j) is equal to H_{ji} (the FRF measured at DOF j due to excitation at DOF i).

Figures 9 and 10 show two examples of the results from investigating this criterion. In both examples the shaker was attached to the normal excitement point and an accelerometer was attached to a bracket near the tip of the blade. This resulted in a FRF with the shaker in the root excitement mode. Then the shaker was moved down to the tip bracket, which was designed to act as the attachment point for the tip excitement mode, and the accelerometer was moved to the original excitement point which resulted in a FRF for the tip excitement mode that should be similar to the first FRF. The two examples shown are for 12.55- and 25.11-Hz flapwise modes. It is easy to see that the frequency, magnitudes (except for sign), and curve shape are similar. The sign reversal in the magnitudes is due to the change in shaker orientation when its location is switched with that of the accelerometer.

The next step was to determine the rigid-body natural frequencies of the blade in the free-free test condition with the shaker detached. The blade motions were excited by hand. The natural frequencies measured are

First Torsional 0.2 Hz
First Flapping 0.8 Hz

Once the linearity of the system and the rigid-body natural frequencies had been confirmed, the shake-test investigation was ready to be started. First, a model of the blade (fig. 11) was constructed. The local origin for the coordinate system was on the leading edge of the unswept portion of the blade in line with the tip. The node points represented the leading and trailing edges of the blade and were spaced along the span every 16 in. except at the root. Nodes 37 and 38 were the shaker attachment points and were not a part of the blade. The accelerometer was placed at each node point for every mode identified. The coordinates of each node are listed in Table 1.

The blade was first excited over a wide band to get an approximate idea of the natural frequency locations. The input frequencies were varied from 3 to 100 Hz with a resolution of 0.08 Hz. Figure 12 shows the results of this excitement for 3 to 35 Hz and figure 13 shows the results of this excitement for 35 to 100 Hz. From these plots, nine frequencies of possible modes were identified. Next, the blade was excited over a narrowband frequency range centered at the frequencies identified in the wideband excitement. The narrowband excitation was then repeated until the response at each of the nodes in the model was measured with the accelerometer. The data from the narrowband excitement were then used to identifiy the natural frequencies, mode shapes, and damping of the blade. A high-resolution narrowband excitement was needed to identify the modes because of the light damping and coupling of some of the modes. The modes that could be considered single-degree-of-freedom modes were identified by a resonance phenomena technique (ref. 4). Modal damping for all modes, and the frequencies of multiple-degree-of-freedom modes, were determined using modal analysis software developed by Structural Measurement Systems.

RESULTS

Table 2 lists frequencies and damping ratios and the type of excitation for the modes investigated. All estimates were made using a single-degree-of-freedom (SDF) model with the exception of the third flapwise and first chordwise modes. A multiple-degree-of-freedom model was used to estimate these parameters. Because of the modal coupling, various modes could be excited by off-axis forcing; chordwise modes were excited by flapwise inputs. The frequencies and damping ratios were slightly affected by the different excitation types. Therefore, it became necessary to list the excitation type which produced the best response.

Table 3 lists the non-rotating natural frequencies calculated by the CAMRAD program (ref. 5). A direct comparison of these frequencies cannot be made because of the differences in boundary conditions. However, by solving the classical free vibration partial differential equation (ref. 6)

$$\frac{\partial^2}{\partial x^2}\left[\mathrm{EI(x)}\frac{\partial^2 y(x,t)}{\partial x^2}\right] = -\mathrm{m}(x)\frac{\partial^2 y(x,t)}{\partial t^2} \tag{1}$$

a ratio can be calculated that relates the natural frequencies for both boundary conditions. Assuming an uniform blade and using the separated variable technique (1) reduces to

$$\frac{d^4 Y(x)}{dx^4} - \beta^4 Y(x) = 0, \qquad \beta^4 = \frac{\omega^2 m}{EI} \tag{2}$$

which has the general solution of

$$Y(x)= C_1 \sin \beta x + C_2 \cos \beta x + C_3 \sinh \beta x + C_4 \cosh \beta x \quad (3)$$

The appropriate boundary conditions for both cases, hinge-free and free-free, are

hinge-free	free-free
$Y(0) = 0,\ \left.\frac{d^2Y}{dx^2}\right\|_{x=L} = 0$	$\frac{d^3Y}{dx^3} = 0 \quad @\ x = 0 \text{ or } x = L$
$\left.\frac{d^2Y}{dx^2}\right\|_{x=0} = 0,\ \left.\frac{d^2Y}{dx^2}\right\|_{x=L} = 0$	$\frac{d^2Y}{dx^2} = 0 \quad @\ x = 0 \text{ or } x = L$

By substituting the boundary conditions into the general solution (3) the problem becomes one of finding the eigenvalues. The resulting frequency equations that must be solved are

$$\cos \beta L \cosh \beta L = 1$$

and

$$\frac{\sin \beta L}{\sinh \beta L} \cosh \beta L - \cos \beta L = 1$$

These equations have an infinite number of solutions, β_r. The solution approaches

$$\beta_r \rightarrow (r + 0.5)\pi \Big|_{r \rightarrow \infty} \lim$$

for the hinge-free case, and

$$\beta_r \rightarrow (r + 0.25)\pi \Big|_{r \rightarrow \infty} \lim$$

for the free-free case as (r) increases. These solutions can then be compared, and the ratios (shown in Table 4) can be calculated. The same comparison can be made between the free-free and the fixed-free boundary conditions for torsional modes. These results are also shown in Table 4. Finally, the natural frequencies calculated by CAMRAD can be multiplied by the free-free/hinge-free ratio and compared directly to the measured natural frequencies (Table 5). It can be seen when comparing values from the measured free-free boundary conditions to values from the calculated free-free boundary conditions that there is very close agreement between the lower modes of the flap and the lag motion. However, the correlation for the higher flapwise and chordwise modes as well as for both torsional modes is very poor. The reason for the poor correlation of these modes is unknown at this time.

Table 6 lists one column of the residue matrix for each mode measured. The nature of the residue matrix requires only one column to identify the full matrix (ref. 7). Data for the column of the residue matrices comes from the imaginary part of the FRF at the resonant frequencies. This column represents the scaled mode shape of each mode. Figure 14 shows plots of these residues. The classical mode shapes for a free-free supported beam are shown in the flapwise and chordwise modes. These plots also show some coupling between the higher-order flapwise and torsional modes. The coupling between the third

flapwise and the first chordwise modes does not show up because the accelerometer does not respond to off-axis motion.

CONCLUSION

The shake test identified five flapwise, two chordwise, and two torsional modes. The measured mode shapes are the classical shapes expected, which gives credibility to the data. The data was compared to CAMRAD data, and there was good agreement for the lower flapwise and chordwise modes but not for the torsional modes and higher-frequency flatwise and chordwise modes. It is recommended that during the next shake test the blade be supported with a hinge-free support to better model the blade/hub attachment for ease of analysis. Further, the data should also be used to calculate mass and stiffness matrices for comparison with input data used in CAMRAD.

REFERENCES

1. Watts, M. E.; and Cross, J. L.: The NASA Modern Technology Rotors Program. AIAA Paper 86-9788, Las Vegas, NV, April 1986.

2. Seto, Edward, I.: NASA/ARMY Black Hawk (UH-60A) Rotor Project Plan, Aug. 1987.

3. Esculier, Jacques; and Bousman, William G.: Calculated and Measured Blade Structural Response on a Full-Scale Rotor. AHS 42nd Annual Forum Proceedings, June 1986, pp. 81-110.

4. Ibrahim, Samir R.: Modal Identification Techniques Assessment and Comparison. Presented at the 3rd International Modal Analysis Conference, Orlando, FL, Jan. 1985.

5. Johnson, Wayne: A Comprehensive Analytical Model of Rotorcraft Aerodynamics and Dynamics, Part I: Analysis Development. NASA TM-81182, June 1980.

6. Meirovitch, Leonard: Analytical Methods in Vibrations. The Macmillan Company, 1967.

7. Richardson, M.; and Potter, R.: Identification of the Modal Properties of an Elastic Structure from Measured Transfer Function Data. Instrument Society of America 20th International Instrumentation Symposium, Albuquerque, NM, 1974.

TABLE 1.– COORDINATES OF BLADE MODEL

Measurement point coordinates, in.			
Pt	x	y	z
1	0.000	27.000	0.000
2	0.000	6.500	0.000
3	0.000	20.500	21.000
4	0.000	0.000	21.000
5	0.000	20.500	37.000
6	0.000	0.000	37.000
7	0.000	20.500	53.000
8	0.000	0.000	53.000
9	0.000	20.500	69.000
10	0.000	0.000	69.000
11	0.000	20.500	85.000
12	0.000	0.000	85.000
13	0.000	20.500	101.000
14	0.000	0.000	101.000
15	0.000	20.500	117.000
16	0.000	0.000	117.000
17	0.000	20.500	133.000
18	0.000	0.000	133.000
19	0.000	20.500	149.000
20	0.000	0.000	149.000
21	0.000	20.500	165.000
22	0.000	0.000	165.000
23	0.000	20.500	181.000
24	0.000	0.000	181.000
25	0.000	20.500	197.000
26	0.000	0.000	197.000
27	0.000	20.500	213.000
28	0.000	0.000	213.000
29	0.000	20.500	229.000
30	0.000	0.000	229.000
31	0.000	20.500	245.000
32	0.000	0.000	245.000
33	0.000	20.500	261.000
34	0.000	0.000	261.000
35	0.000	20.500	277.000
36	0.000	0.000	277.000
37	0.000	0.000	287.000
38	0.000	-12.000	287.000

TABLE 2.– FREQUENCIES, DAMPING RATIOS, AND DIRECTION OF EXCITATION FOR MODES IDENTIFIED

Mode	Frequency, Hz	Damping, % cr.	Excitation type
1st Flapwise	4.34	0.27	torsional
2nd Flapwise	12.55	0.09	torsional
3rd Flapwise	24.99	0.12	torsional
4th Flapwise	41.63	0.14	flapwise
5th Flapwise	63.71	0.16	flapwise
1st Torsional	44.55	0.10	torsional
2nd Torsional	82.44	0.21	flapwise
1st Chordwise	25.40	0.24	chordwise
2nd Chordwise	67.38	0.14	chordwise

TABLE 3.– NONROTATING BLADE FREQUENCIES CALCULATED BY CAMRAD (Hz)

Coupled flapwise/chordwise modes Hinge-free constraints
3.21 10.33 17.91 21.92 37.65 52.98 106.11
Torsional modes Fixed-free constraints
23.15 75.42

TABLE 4.– RATIO OF NATURAL FREQUENCIES FOR HINGE-FREE/FREE-FREE SUPPORTS FOR A UNIFORM BEAM

Flapwise modes Chordwise modes	Torsional modes
1.455 1.234 1.163 1.124 1.09	4.00 1.77

TABLE 5.– COMPARISON OF MEASURED VS CALCULATED NATURAL FREQUENCIES (Hz)

Measured	Calculated
Flapwise	
4.34 12.55 24.99 41.63 63.71	4.67 12.75 25.49 42.32 57.75
Chordwise	
25.4 67.71	26.05 65.38
Torsional	
44.55 82.44	92.6 134.07

TABLE 6A.– MODAL RESIDUES, 1ST FLAPWISE[a]

Node	Residue
1	2.443
2	1.520
3	1.605
4	1.046
5	0.870
6	0.864
7	0.340
8	0.259
9	–0.113
10	–0.259
11	–0.468
12	–0.587
13	–0.932
14	–0.986
15	–1.370
16	–1.164
17	–1.336
18	–1.407
19	–1.409
20	–1.361
21	–1.611
22	–1.349
23	–1.362
24	–1.291
25	–1.198
26	–1.024
27	–0.843
28	–0.776
29	–0.480
30	–0.484
31	0.369
32	–0.108
33	0.358
34	0.370
35	0.932
36	0.858
37	1.319
38	–1.059

[a]Mode: 1; Freq.: 4.340 Hz; Damping: 0.27%

TABLE 6B.– MODAL RESIDUES, 2ND FLAPWISE[a]

Node	Residue
1	–1.810
2	–2.692
3	–0.610
4	–1.413
5	0.440
6	–0.262
7	1.339
8	0.661
9	2.256
10	1.392
11	2.500
12	1.857
13	2.490
14	1.718
15	2.210
16	1.485
17	1.420
18	0.766
19	0.600
20	–0.115
21	–0.265
22	–0.955
23	–1.015
24	–1.773
25	–1.441
26	–2.153
27	–1.722
28	–2.219
29	–1.454
30	–2.192
31	–0.852
32	–1.595
33	0.032
34	–0.721
35	1.053
36	0.499
37	1.068
38	–1.178

[a]Mode: 2; Freq.: 12.550 Hz; Damping: 0.09%

TABLE 6C.– MODAL RESIDUES, 3RD FLAPWISE[a]

Node	Residue
1	4.040
2	3.530
3	0.976
4	0.726
5	–0.710
6	–0.802
7	–1.864
8	–1.940
9	–2.240
10	–2.153
11	–1.736
12	–1.605
13	–0.705
14	–0.407
15	0.614
16	0.926
17	1.589
18	1.982
19	2.175
20	2.525
21	1.715
22	2.220
23	0.552
24	1.297
25	–0.856
26	0.076
27	–2.294
28	–1.029
29	–3.217
30	–1.772
31	–3.389
32	–1.710
33	–2.245
34	–0.913
35	–0.895
36	0.572
37	0.741
38	–2.132

[a]Mode: 3; Freq.: 24.99 Hz; Damping: 0.120%

TABLE 6D.– MODAL RESIDUES, 4TH FLAPWISE[a]

Node	Residue
1	3.140
2	2.356
3	1.660
4	–0.527
5	0.393
6	–1.319
7	0.005
8	–1.425
9	0.416
10	–0.724
11	1.530
12	0.306
13	1.602
14	1.132
15	1.408
16	1.351
17	0.425
18	0.874
19	–0.966
20	0.035
21	–2.306
22	–0.700
23	–2.219
24	–0.936
25	–2.763
26	–0.420
27	–1.862
28	0.534
29	–1.013
30	1.521
31	–0.706
32	1.960
33	–1.250
34	1.642
35	–2.210
36	0.698
37	0.414

[a]Mode: 4; Freq.: 41.63 Hz; Damping: 0.140%

TABLE 6E.– MODAL RESIDUES, 5TH FLAPWISE[a]

Node	Residue
1	–2.500
2	–2.983
3	1.250
4	–0.078
5	3.040
6	1.042
7	2.880
8	0.681
9	1.190
10	–0.718
11	–0.408
12	–1.870
13	–0.498
14	–1.774
15	0.830
16	–0.559
17	2.349
18	0.888
19	2.681
20	1.466
21	1.243
22	0.783
23	–1.081
24	–0.636
25	–2.641
26	–1.497
27	–2.510
28	–1.074
29	–1.060
30	0.370
31	0.419
32	1.691
33	0.258
34	1.829
35	–1.077
36	0.659
37	0.709

[a]Mode: 5; Freq.: 63.715 Hz; Damping: 0.16%

TABLE 6F.– MODAL RESIDUES, 1ST CHORDWISE[a]

Node	Residue
1	1.864
2	–1.635
3	1.277
4	–1.191
5	0.828
6	–0.639
7	0.371
8	–0.244
9	–0.078
10	0.216
11	–0.603
12	0.605
13	–0.922
14	0.833
15	–1.213
16	0.977
17	–1.377
18	1.077
19	–1.426
20	1.090
21	–1.374
22	1.007
23	–1.151
24	0.912
25	–0.955
26	0.854
27	–0.666
28	0.719
29	–0.358
30	0.485
31	0.011
32	0.144
33	0.397
34	–0.212
35	0.742
36	–0.817
37	–0.943

[a]Mode: 1; Freq.: 25.38 Hz; Damping: 0.25%

TABLE 6G.– MODAL RESIDUES, 2ND CHORDWISE[a]

Node	Residue
1	–3.494
2	3.438
3	–2.001
4	1.606
5	–0.130
6	0.083
7	1.220
8	–1.286
9	2.190
10	–2.288
11	2.770
12	–2.745
13	2.657
14	–2.640
15	2.091
16	–2.125
17	1.178
18	–1.220
19	0.006
20	0.113
21	–1.110
22	1.265
23	2.095
24	2.185
25	–2.701
26	2.720
27	–2.883
28	2.910
29	–2.625
30	2.647
31	–1.924
32	1.861
33	–0.834
34	0.756
35	0.573
36	–0.731
37	–2.194

[a]Mode: 2; Freq.: 67.380 Hz; Damping: 0.14%

TABLE 6H.– MODAL RESIDUES, 1ST TORSIONAL[a]

Node	Residue
1	26.710
2	–6.530
3	21.760
4	–8.330
5	26.860
6	–2.460
7	28.260
8	0.322
9	22.930
10	0.186
11	15.360
12	–3.040
13	6.500
14	–7.350
15	–0.869
16	–9.334
17	–4.070
18	–7.320
19	–2.920
20	–1.720
21	–0.707
22	4.528
23	–0.318
24	9.010
25	–4.820
26	11.480
27	–13.213
28	7.930
29	–21.975
30	3.483
31	–26.415
32	0.836
33	–32.494
34	1.490
35	–25.422
36	6.070
37	5.934
38	–20.290

[a]Mode: 1; Freq.: 44.550 Hz; Damping: 0.100%

TABLE 6I.– MODAL RESIDUES, 2ND TORSIONAL[a]

Node	Residue
1	–6.600
2	–1.965
3	–0.636
4	0.965
5	0.640
6	0.685
7	0.358
8	–0.485
9	0.288
10	–1.359
11	1.520
12	–1.148
13	3.366
14	–0.231
15	4.500
16	0.260
17	3.820
18	–0.306
19	1.960
20	–1.370
21	0.595
22	–1.926
23	0.797
24	–1.129
25	1.757
26	0.256
27	1.849
28	1.128
29	0.161
30	0.804
31	–2.261
32	–0.059
33	–3.315
34	–0.288
35	–2.965
36	0.421
37	–0.916

[a]Mode: 2; Freq.: 82.550 Hz; Damping: 0.21%

Figure 1.– Supported UH-60 blade.

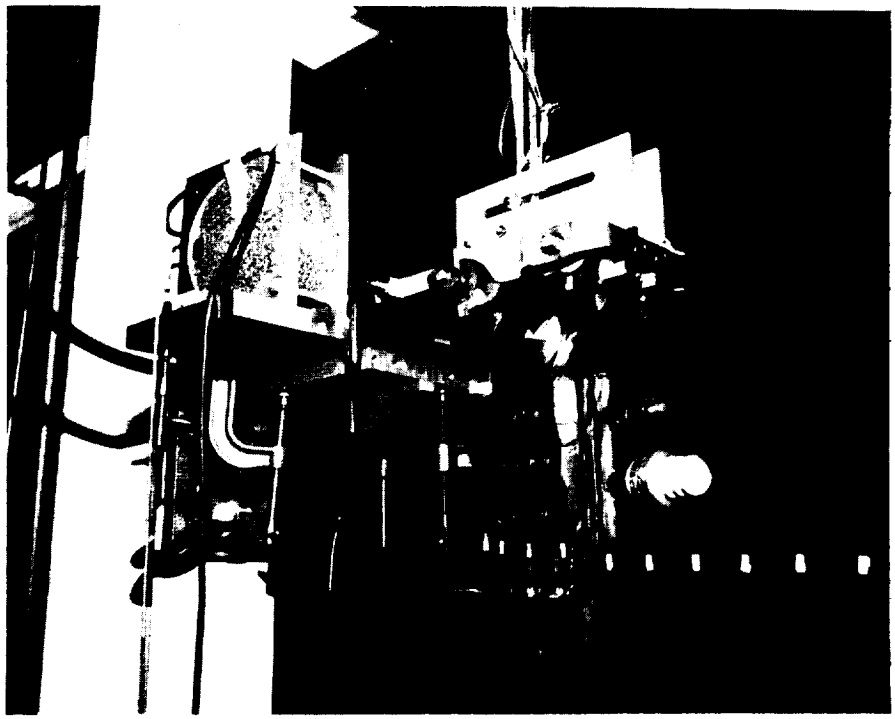

Figure 2.– UH-60 blade, bungee cords, and shaker.

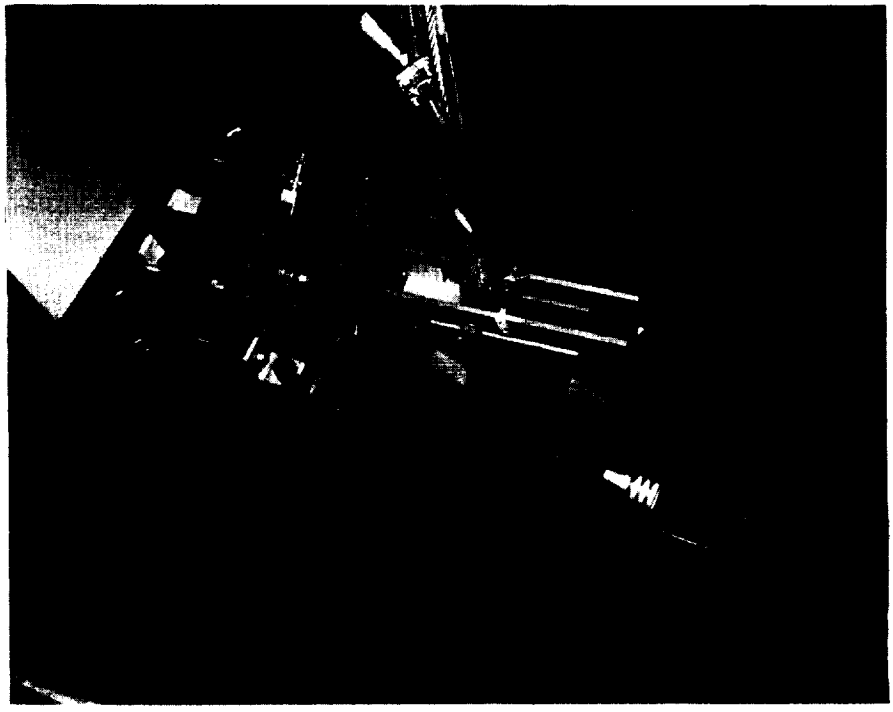

Figure 3.– UH-60 blade and shaker in chordwise excitation mode.

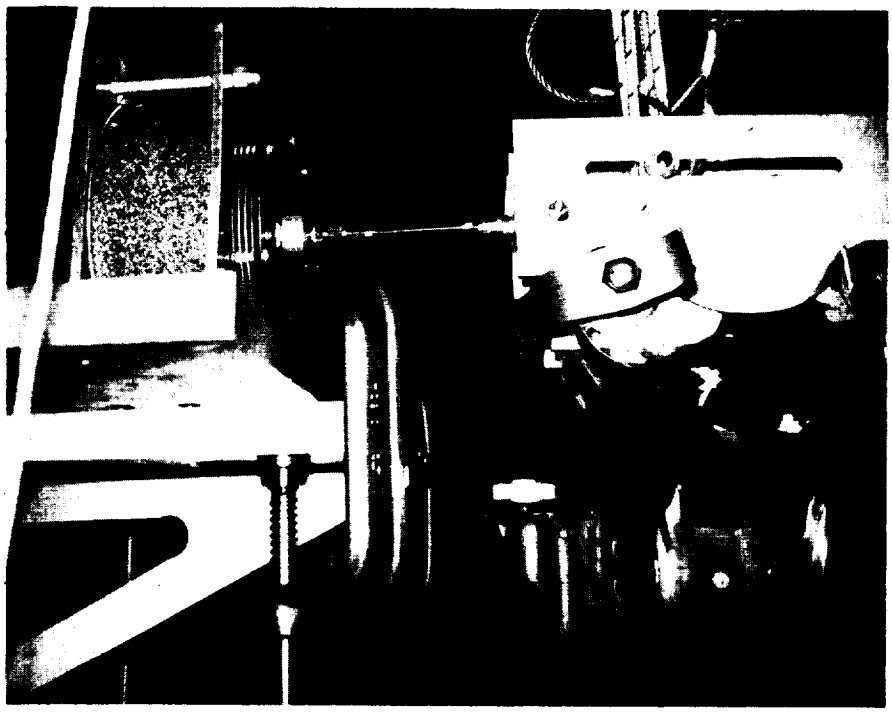

Figure 4.– UH-60 blade and shaker in chordwise excitation mode.

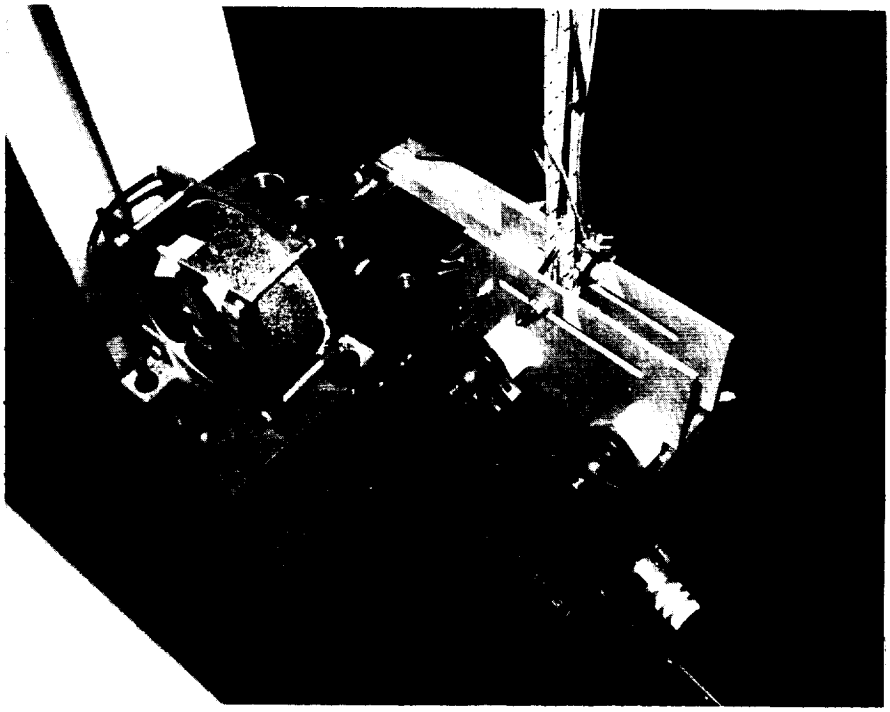

Figure 5.– UH-60 blade and shaker in torsional excitation mode.

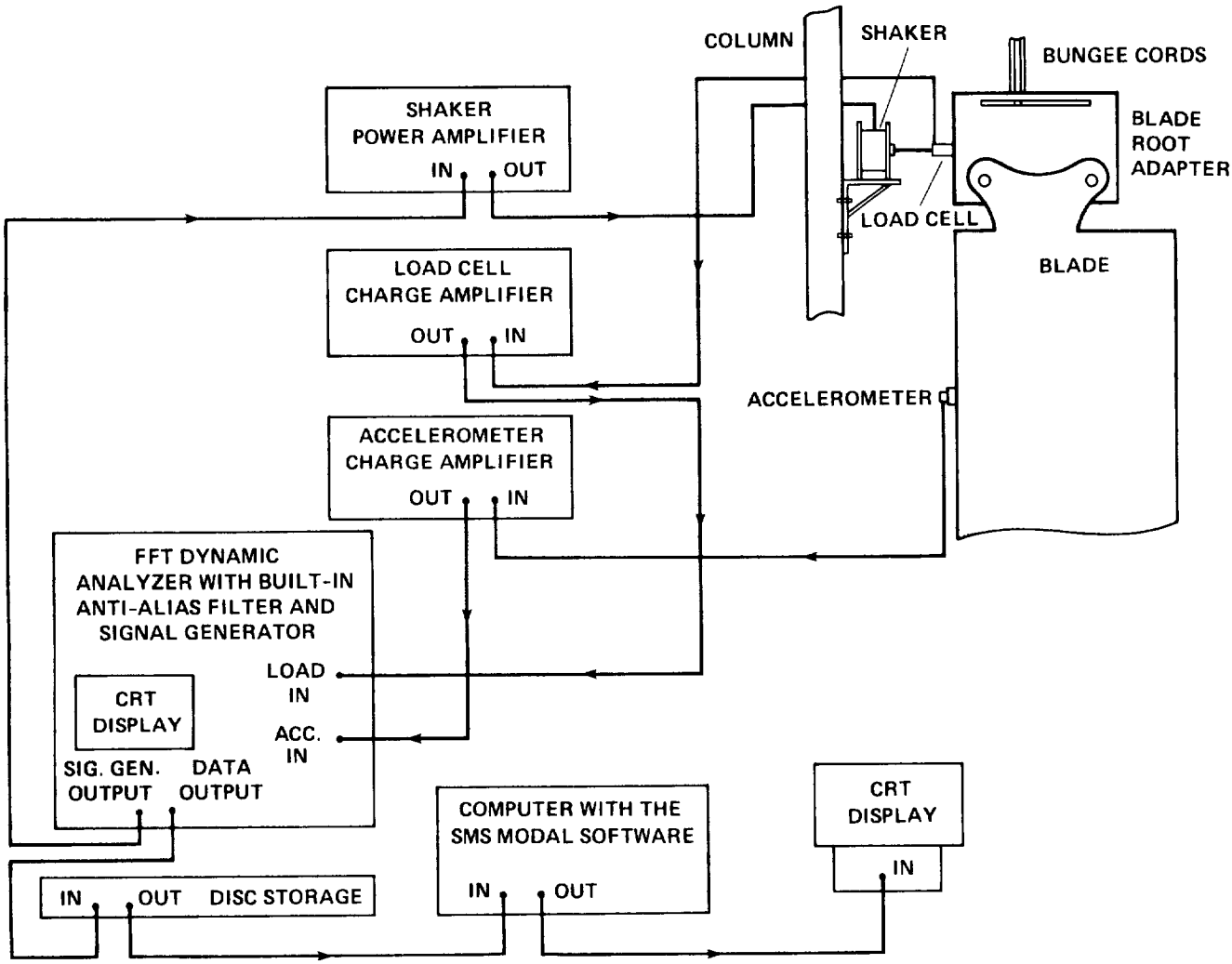

Figure 6.– Test setup schematic.

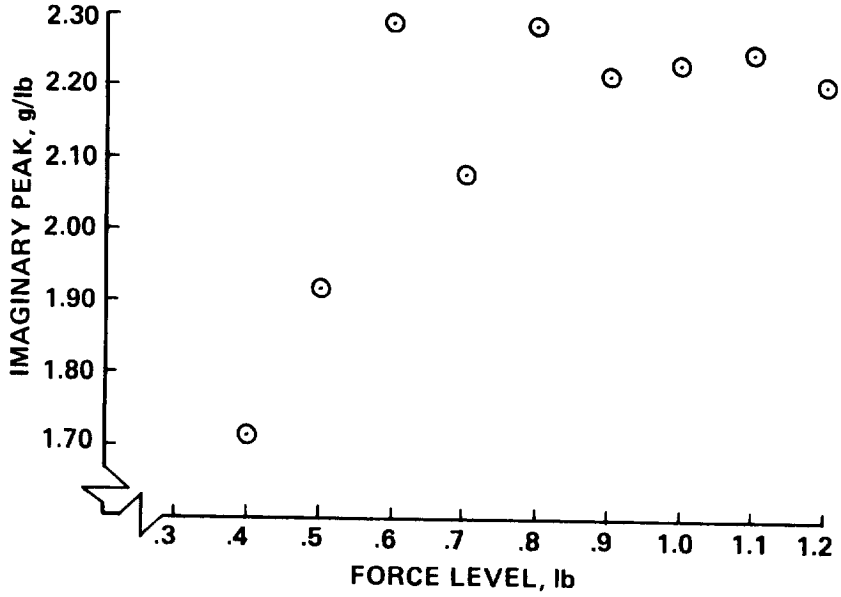

Figure 7.– Imaginary peak of frequency response function vs input level.

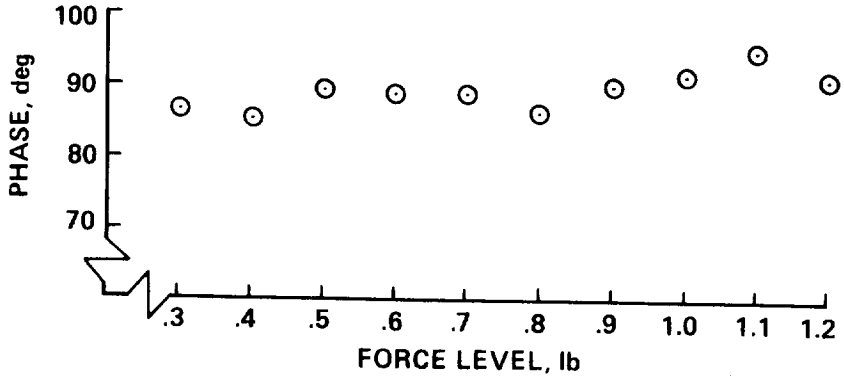

Figure 8.– Phase of frequency response function vs input excitement level.

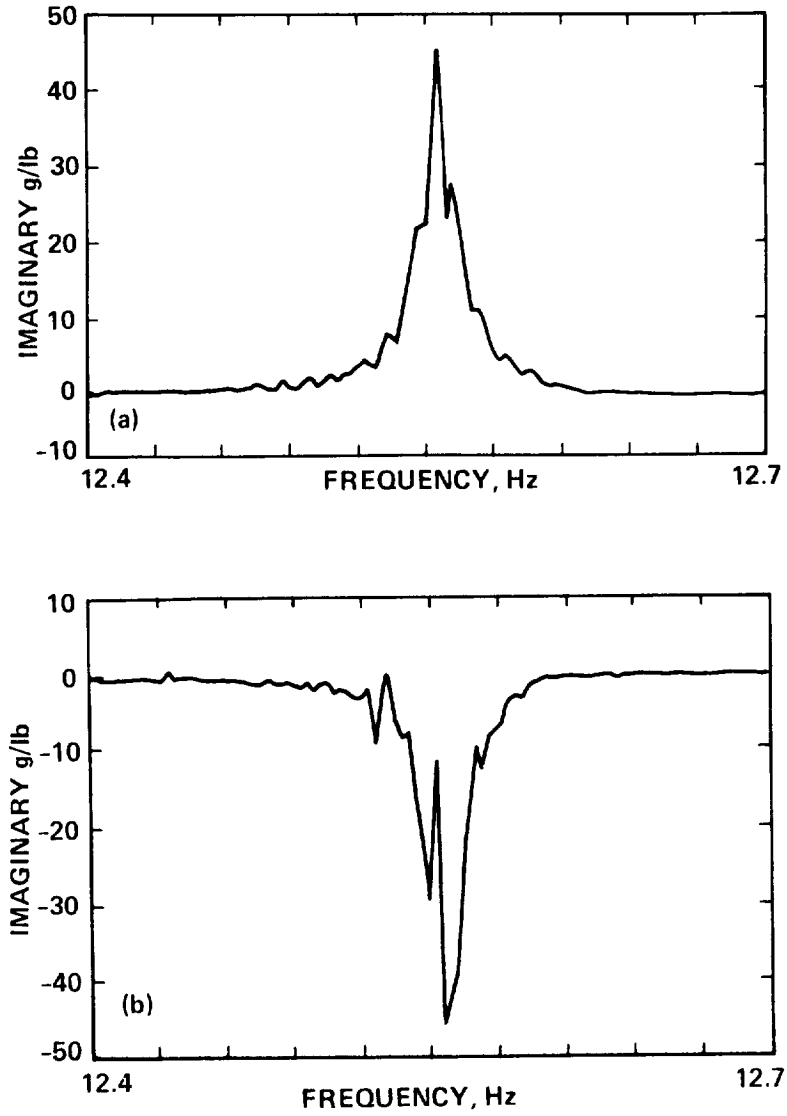

Figure 9.– Flapwise reciprocity test, 12.55 Hz. (a) Exciting force near tip, (b) exciting force near root.

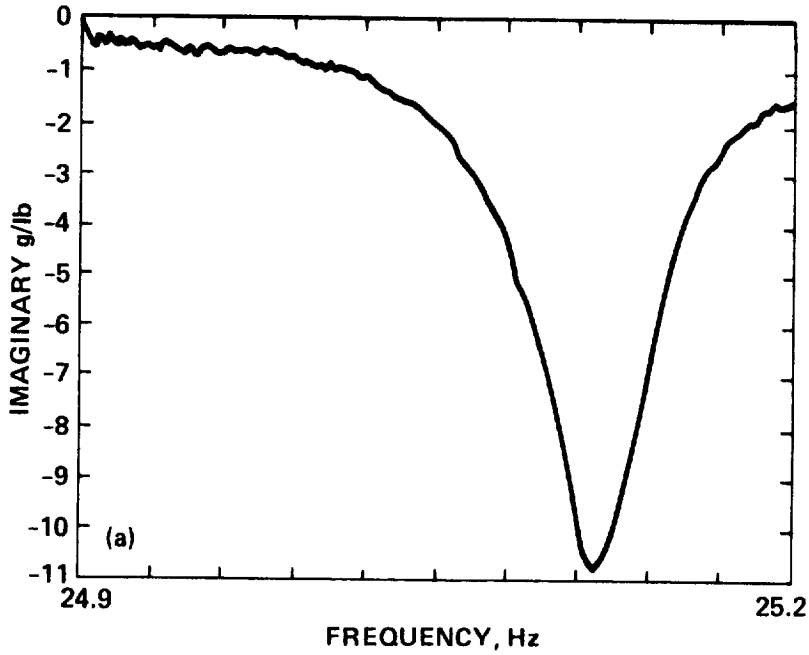

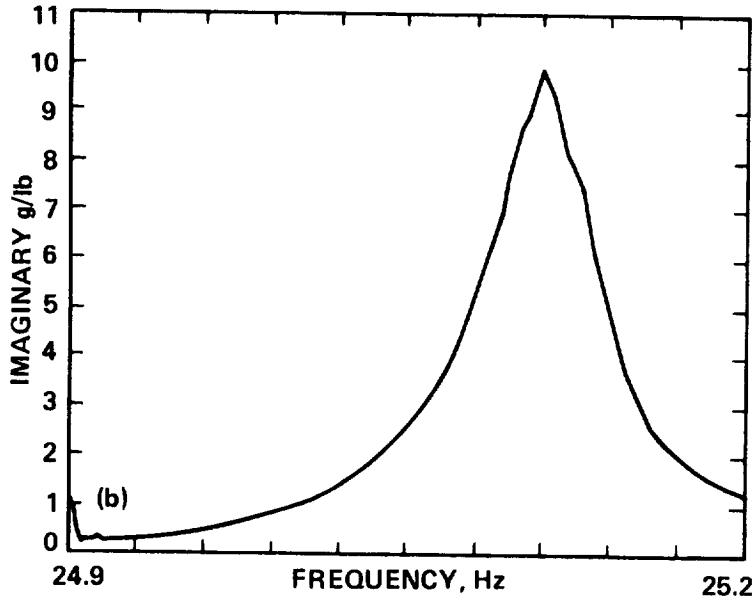

Figure 10.– Flapwise reciprocity test, 25.10 Hz. (a) Exciting force near tip, (b) exciting force near root.

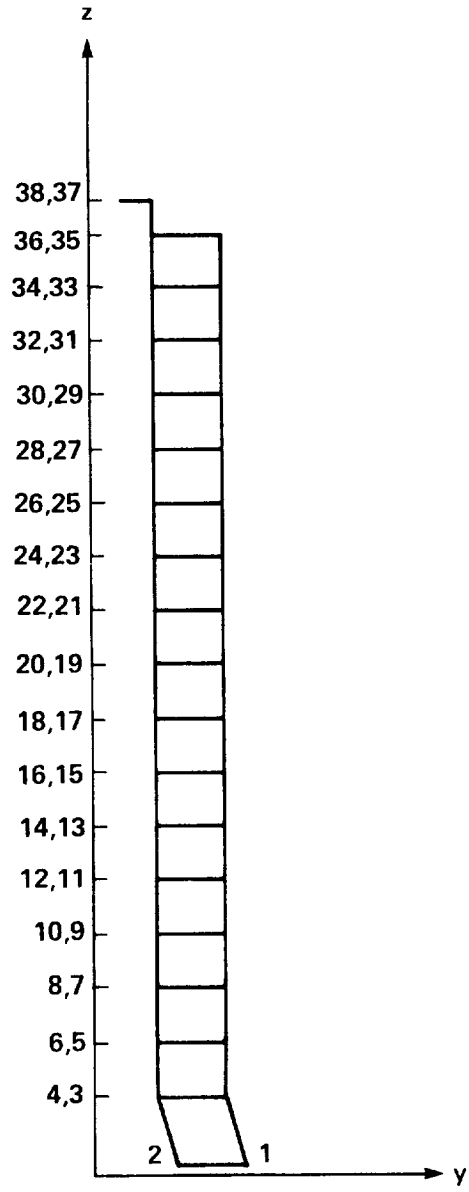

Figure 11.– UH-60 blade model, showing node points at which the accelerometer was placed.

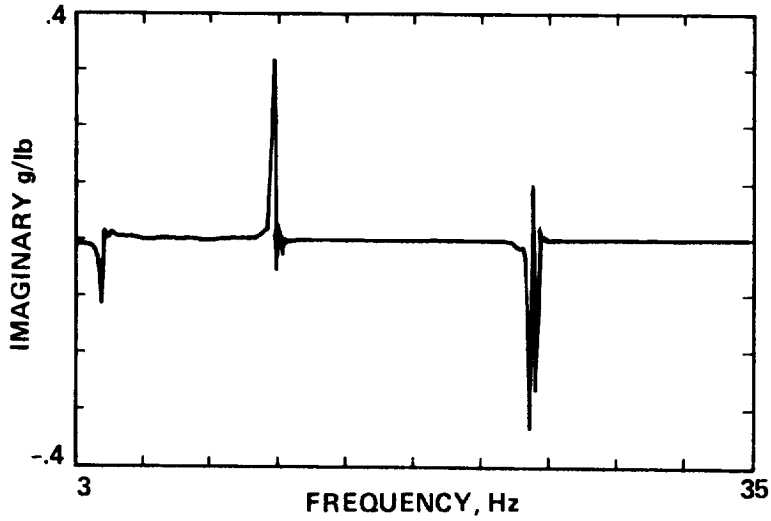

Figure 12.– UH-60 blade frequency response function of wideband excitation between 3 and 35 Hz.

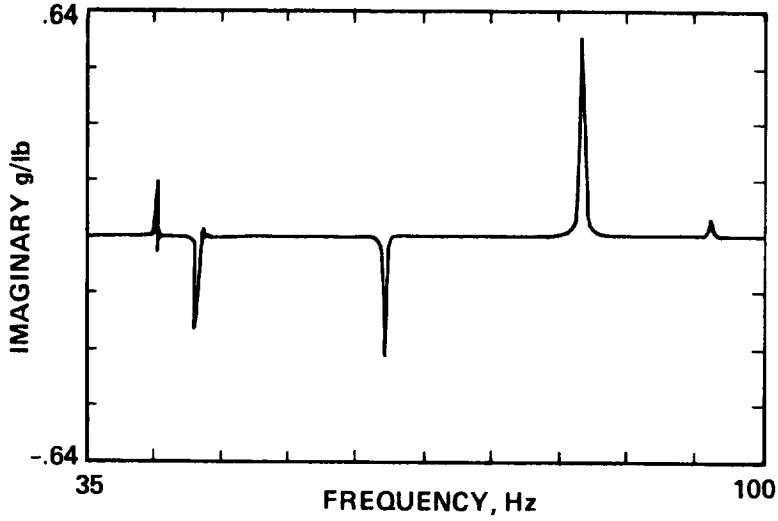

Figure 13.– Frequency response function of wideband excitation between 35 and 100 Hz.

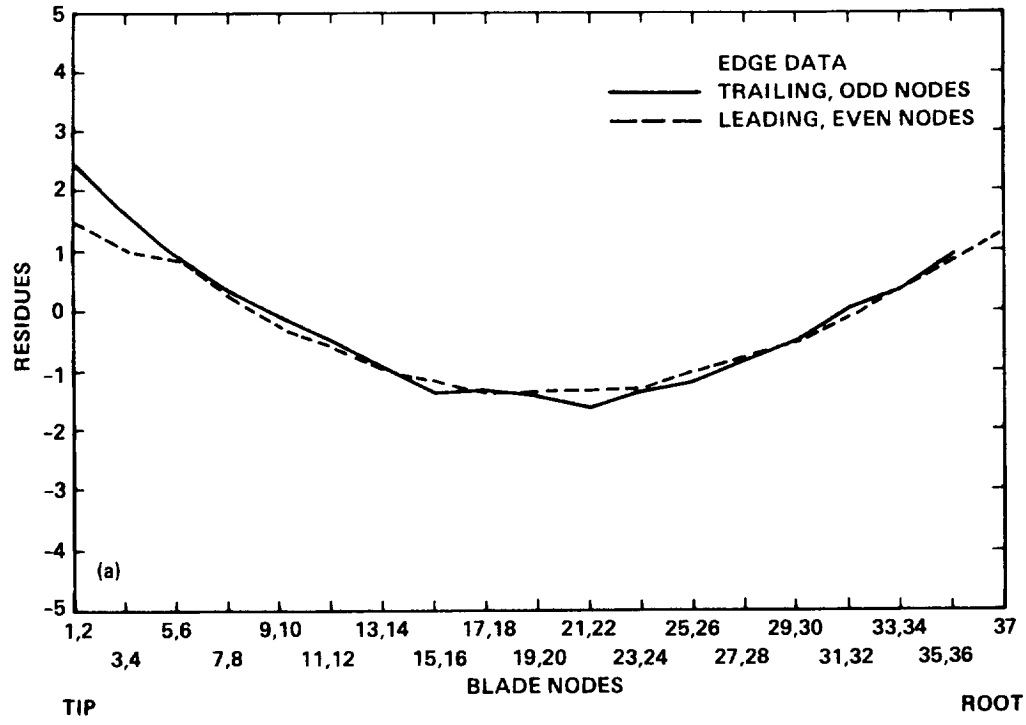

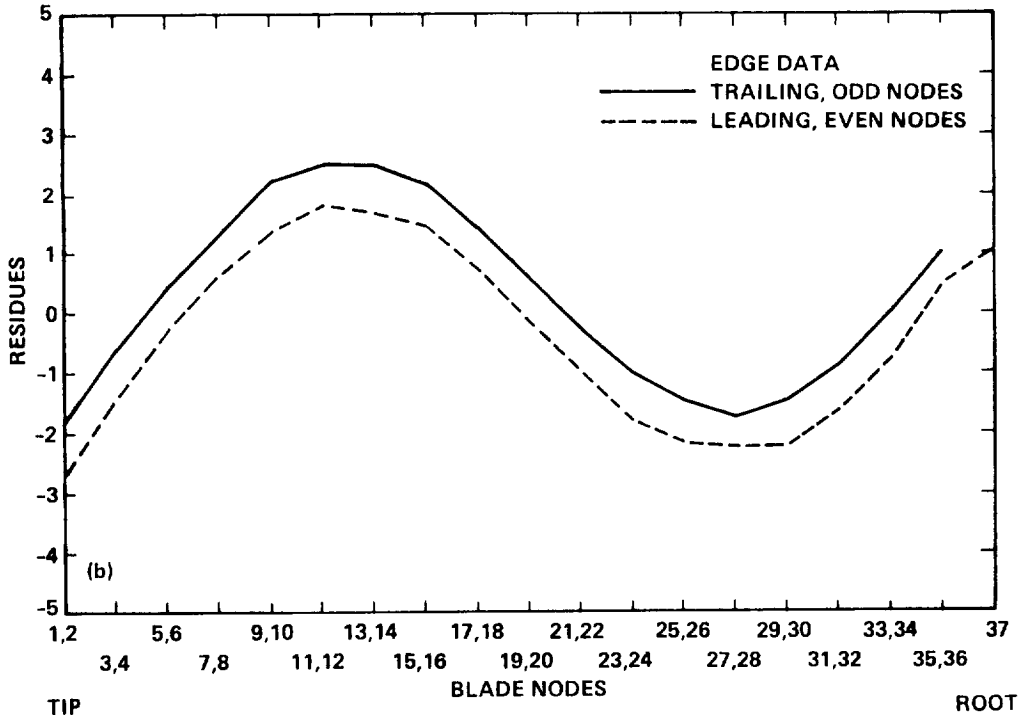

Figure 14.– UH-60 blade residue vs blade nodes. (a) 1st flapwise, (b) 2nd flapwise.

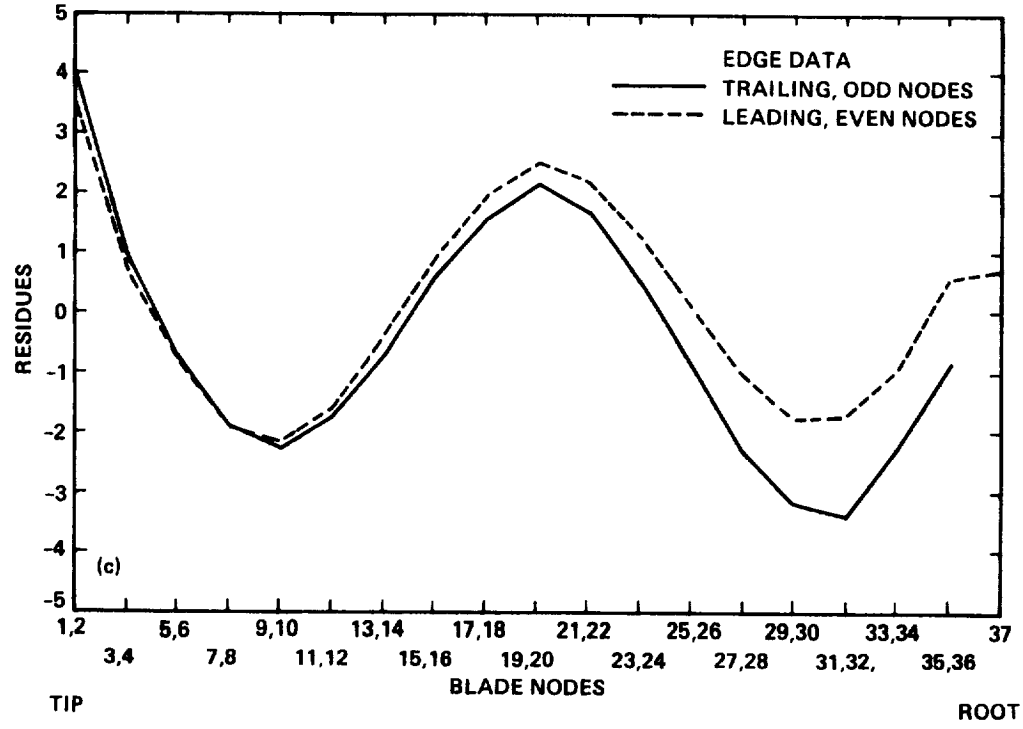

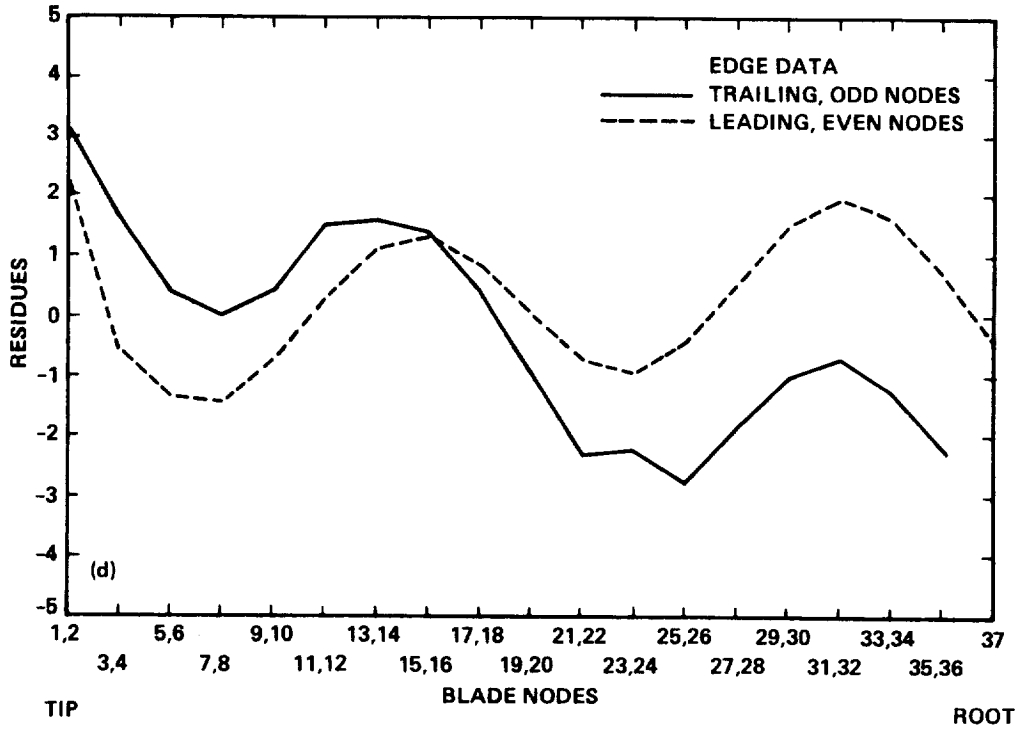

Figure 14.– Continued. (c) 3rd flapwise, (d) 4th flapwise.

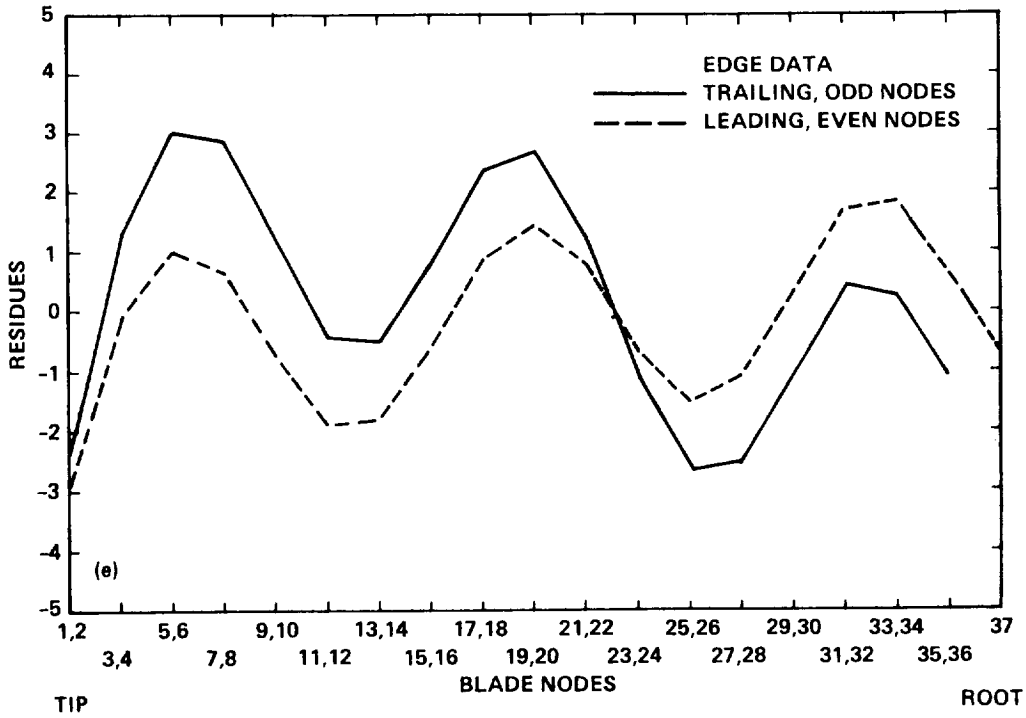

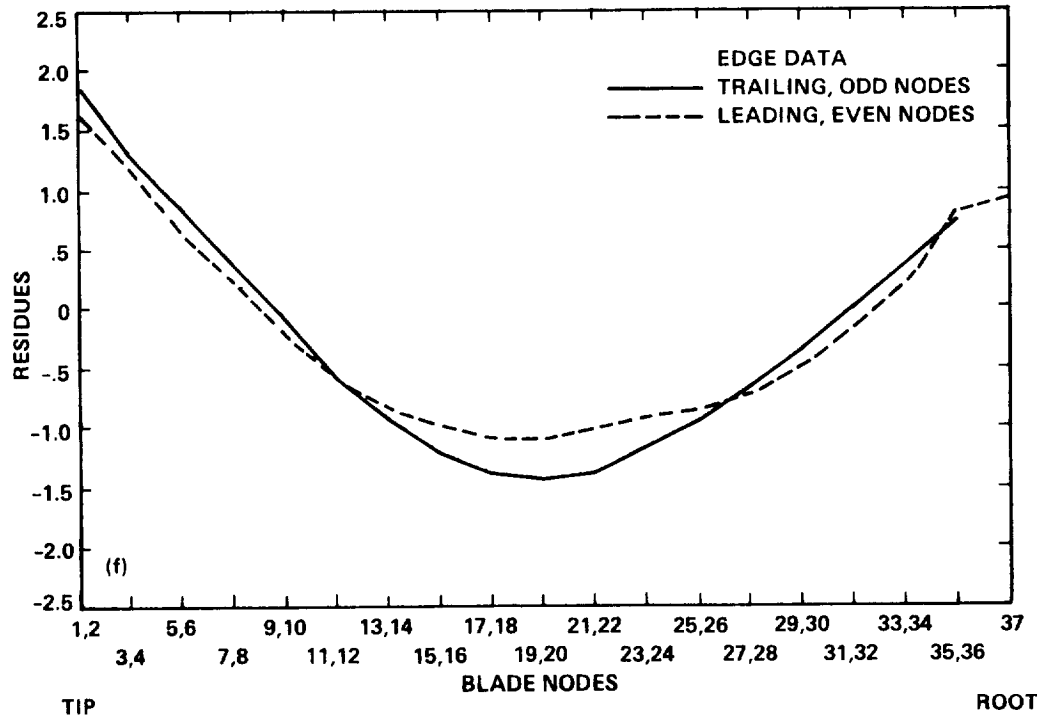

Figure 14.– Continued. (e) 5th flapwise, (f) 1st edgewise.

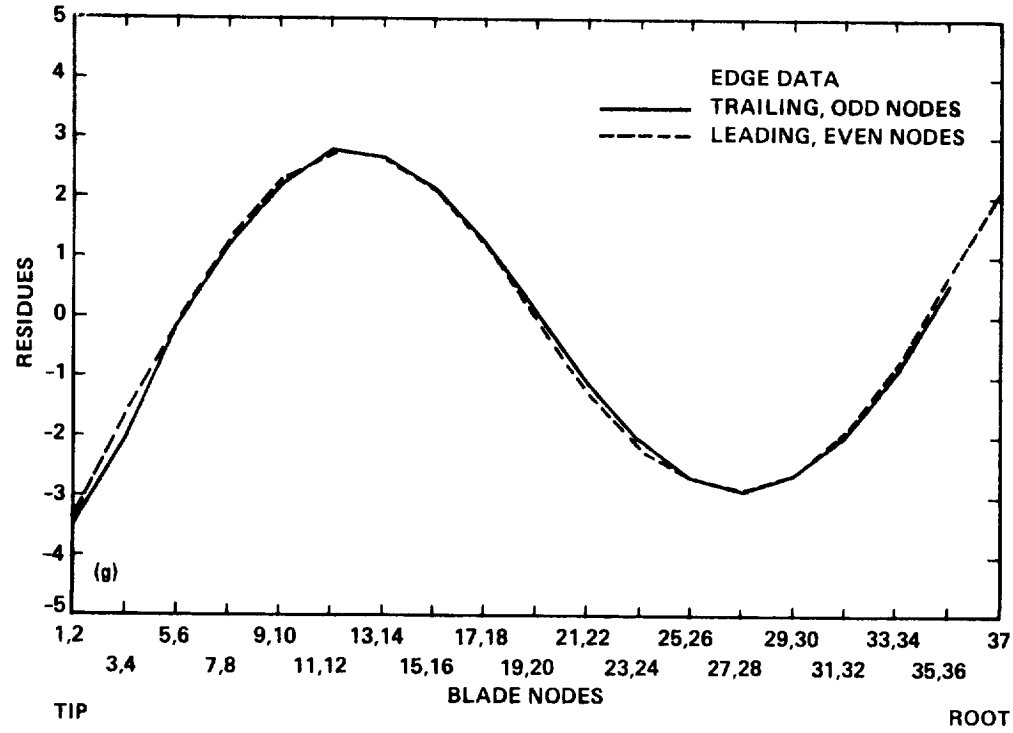

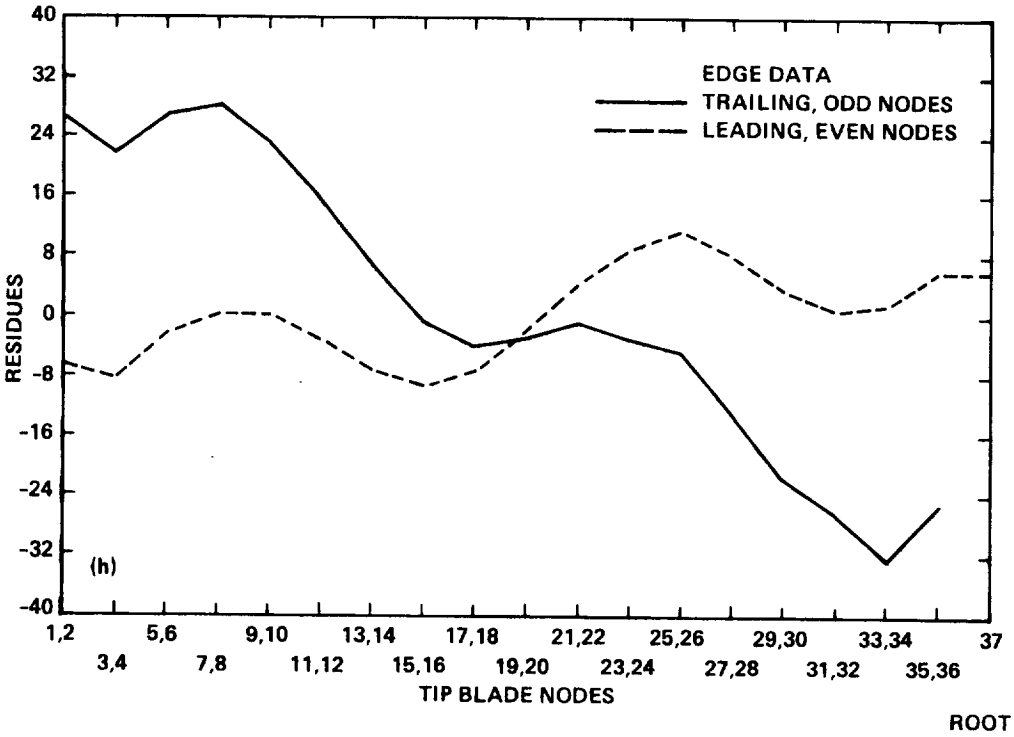

Figure 14.– Continued. (g) 2nd edgewise, (h) 1st torsional.

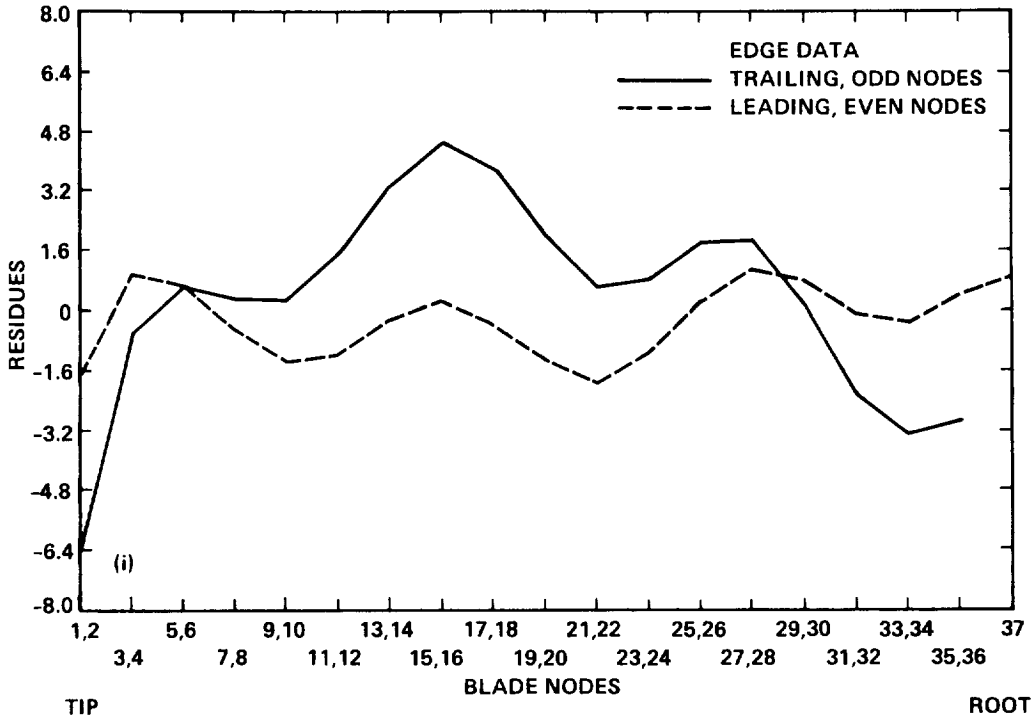

Figure 14.– Concluded. (i) 2nd torsional.

NASA
National Aeronautics and Space Administration

Report Documentation Page

1. Report No.	2. Government Accession No.	3. Recipient's Catalog No.
NASA TM-101005		

4. Title and Subtitle	5. Report Date
Full-Scale UH-60A Rotor Blade Nonrotating Modal Analysis Shake Test	November 1989
	6. Performing Organization Code
7. Author(s)	8. Performing Organization Report No.
Robert M. Kufeld and David Nguyen	A-88198
	10. Work Unit No.
	505-42-51
9. Performing Organization Name and Address	11. Contract or Grant No.
Ames Research Center Moffett Field, CA 94035	
12. Sponsoring Agency Name and Address	13. Type of Report and Period Covered
National Aeronautics and Space Administration Washington, DC 20546-0001	Technical Memorandum
	14. Sponsoring Agency Code

15. Supplementary Notes

Point of Contact: Robert M. Kufeld, Ames Research Center, MS 237-5, Moffett Field, CA 94035
(415) 694-4682 or FTS 464-4682

16. Abstract

This report documents the test procedures and results of a nonrotating modal analysis shake test of a full-scale UH-60A rotor blade. The test was performed at NASA Ames Research Center during April of 1986. Five flatwise, two torsional, and two chordwise modes were measured. The frequencies ranged between 4.35 and 82.44 Hz. The results were compared to the natural frequencies calculated by the Comprehensive Analytical Model of Rotorcraft Aerodynamics and Dynamics simulation program. The results will be used to verify mass and stiffness input data for various simulation programs.

17. Key Words (Suggested by Author(s))	18. Distribution Statement
Rotor blade Dynamic test Mode shapes	Unclassified-Unlimited Subject Category - 09

19. Security Classif. (of this report)	20. Security Classif. (of this page)	21. No. of Pages	22. Price
Unclassified	Unclassified	36	A03